Calibration and Weather Observation of a Dual-polarized Phased Array Line Replaceable Unit Radar Demonstrator

Pei-sang Tsai
Earth Observing Lab., NCAR
Boulder, Colorado
ptsai@ucar.edu

Rodrigo M. Lebrón
ARRC, University of Oklahoma
Norman, Oklahoma
rodrigolebron@ou.edu

Jonathan M. Emmett
Earth Observing Lab., NCAR
Boulder, Colorado
jemmett@ucar.edu

Adam Karboski
Earth Observing Lab., NCAR
Boulder, Colorado
karboski@ucar.edu

Christopher Burghart
Earth Observing Lab., NCAR
Boulder, Colorado
burghart@ucar.edu

Jorge Salazar
ARRC, University of Oklahoma
Norman, Oklahoma
salazar@ou.edu

Scott Ellis
Earth Observing Lab., NCAR
Boulder, Colorado
sellis@ucar.edu

James Ranson
Earth Observing Lab., NCAR
Boulder, Colorado
jranson@ucar.edu

Eric Loew
Earth Observing Lab., NCAR
Boulder, Colorado
ericloew@ucar.edu

***Abstract*—This paper provides an overall, detailed description of a C-band, 64-element Line Replaceable Unit (LRU) radar system. The LRU radar system was developed as a technology demonstrator to explore various phased array related technologies and investigate the technical requirements for the next-generation airborne phased array radar (APAR). The demonstrator served as a research platform through various calibration related topics, beamforming, and expansion to an end-to-end radar system.**

***Index Terms*—Line replaceable unit, APAR, dual polarization, calibration, beamforming, mutual coupling, embedded element pattern**

I. Introduction

The National Center for Atmospheric Research (NCAR) is currently investigating the technical requirements for the next-generation airborne phased array radar (APAR). This airborne radar system will be used to retrieve dynamic and microphysical characteristics of clouds and precipitation [1]. Phased array radar (PAR) characteristics such as side lobe level (SLL), gain and beam accuracy are critical to the weather observation requirements [2]–[4]. In 2015, NCAR began building a PAR technology demonstrator to serve as a research and development platform for APAR. This C-band, dual-polarized, 64 element active electronically scanned array (AESA), designated the Line Replaceable Unit (LRU) Demonstrator, underwent a series of calibration efforts. The LRU Demonstrator was later expanded into a fully operational radar system incorporating beam-steering, and real-time signal processing and display. Various engineering challenges and limitations were discovered while developing the LRU Demonstrator. This experience was invaluable and reduced risk considerably for the APAR development.

To ensure the correct performance of the radar, it is essential to develop a calibration scheme for a PAR system. While the conventional method of using an anechoic chamber is the baseline of any PAR calibration, the development of a self-calibration method [5] will provide essential calibration capability once the system is fielded on the aircraft. Calibration during field operations will only allow minimal infrastructure and equipment. To comply with this limitation, mutual coupling-based approaches were recently investigated [6]. The LRU Demonstrator served as a development platform through this investigation.

Section II provides an overview of the system development and hardware details of the LRU Demonstrator. The requirements related to the mutual coupling-based techniques are also explained and emphasized. The conventional initial calibration results of the Demonstrator are presented in Section III, along with a description of antenna array pattern prediction using the embedded element patterns. Last, sample weather observations using LRU Demonstrator are showcased in Section IV. The weather observations demonstrate end-to-end functionality of the LRU.

This work was supported by the National Oceanic and Atmospheric Administration (NOAA) though the Oceanic and Atmospheric Research (OAR) Office of Weather and Air Quality (OWAQ) under Grants NA170AR110333 and NA18OAR4590431. Additional support is provided from the National Science Foundation (NSF) who funds NCAR under Cooperative Agreement AGS-1852977.

978-1-7281-8942-0/20/$31.00 ©2020 IEEE

II. System Description

A. System Overview

Figure 1 displays a block diagram of the LRU Demonstrator. The system is divided into two main subsystems: front-end and back-end. The front-end consists of the LRU assembly, the radio frequency (RF) transceiver and the Array Controller. The back-end consists of the digital transceiver, time series data acquisition, radar moments generation, real-time display, and time series and moments archiving. In addition to front-end and back-end hardware and software, a mechanical infrastructure, including a radome, was designed and fabricated to house all the components and enable the system to be installed on the NCAR/EOL rooftop testing facility to collect weather data.

The LRU assembly includes the 8x8 planar array antenna, eight transmit/receive module printed circuit boards (T/R module PCBs) shown in the cyan box at the top of Fig. 1, and the associated analog combiners. Each T/R module PCB consists of eight dual-polarization T/R modules arranged in an alternate-transmit, alternate-receive (ATAR) configuration. The T/R modules were designed using commercial-off-the-shelf (COTS) components [7]–[9]. Each T/R module channel is equipped with a 6-bit phase shifter (PS) and a 6-bit attenuator (ATT), and transmits 4 watts of peak power. On-board Wilkinson combiner/dividers provide the common transmit and receive paths required for mutual coupling measurements. The transmit, receive, and test paths of the eight T/R module PCBs are then externally combined using three COTS, balanced, 1-to-8 combiner/dividers. These combiner/dividers form the analog beamforming architecture for the LRU [7]. Figure 2 depicts the 8x8 array element positions and the T/R module PCBs construction. Each PCB is oriented horizontally with the on-board Wilkinson combiner/divider. The COTS 1-to-8 combiner combines each row into one LRU analog channel.

The RF transceiver interfaces the analog beamformer to the back-end. It down-converts the COM_RX and COM_TEST outputs (for Tx monitoring) to intermediate frequencies (IFs) and up-converts the COM_TX input to RF. It provides sufficient bandwidth and frequency discrimination for a combined 40μs Non-linear Frequency Modulated (NLFM) pulse and 1μs single frequency pulse. The long pulse maximizes sensitivity and the short pulse enables near range recovery.

The Array Controller configures phase, amplitude, polarization and transmit states of the T/R modules, and generates the system synchronization signals. To ensure proper synchronization between the digital transceiver and Array Controller, all frequency references are phase-locked to a GPS-disciplined 10 MHz reference. In addition, a transmit qualifier signal (TQS) provides timing synchronization every PRT. Calibration parameters and array beam tables are stored in the T/R module FPGAs.

The LRU host computer houses the digital transceiver and associated data acquisition, radar product generation, display, and archiver software. The digital transceiver provides transmit waveform generation and digital-to-analog conversion to deliver the transmitter excitation signal, and the analog-to-digital conversion (ADC) of the received signals. With the sampling configurations used during LRU radar operation, time series data rates were roughly 25 Mbytes/s each for the long-pulse and short-pulse, or a total time series data rate of about 50 Mbytes/s. Low-level radar products, such as reflectivity, velocity, and spectrum width, also known as moments, are generated and displayed in real-time.

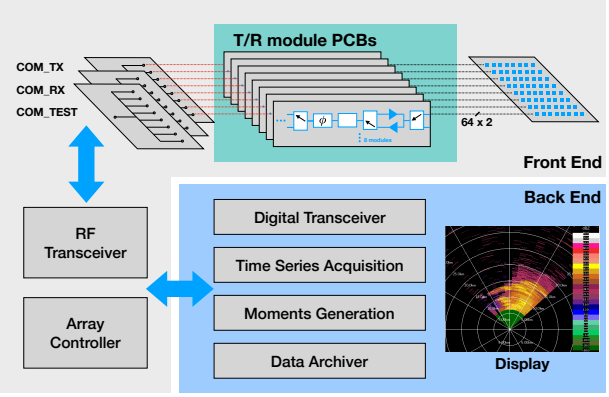

Fig. 1. The system diagram of the LRU-based radar system. The radar system utilizes analog beamforming by employing two levels of analog combiners into one single receive channel. Inversely, dividing one analog transmit channel into 64-element arrav.

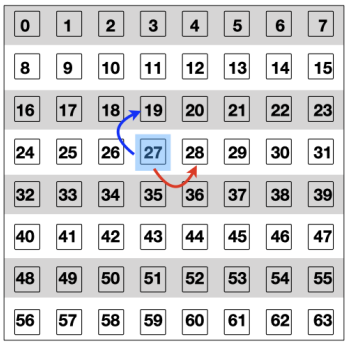

Fig. 2. The 8x8 array element positions. For mutual coupling investigation, Element 27 was selected as the transmit element, while Element 19 and 28 were the receive elements.

B. Mutual Coupling Capable Hardware

The mutual coupling technique requires T/R module elements to have independent transmit and receive capability. The independent analog beamformers and individually controlled T/R modules are two essential requirements. While one T/R module is commanded to transmit, the rest of the modules will be in receive mode to measure the mutual coupling effects. Fig. 3 depicts a T/R module front-end diagram. Assuming the top module transmits full power and the bottom module is in receive mode. The worst case mutual coupling measurements will likely to occur to two adjacent elements. With a nominal

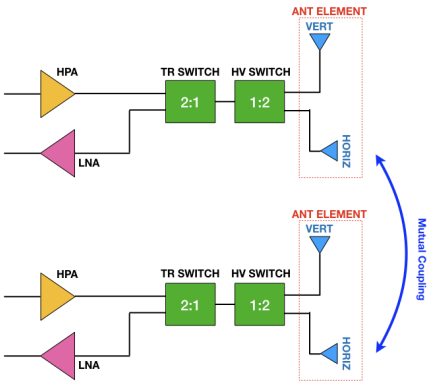

Fig. 3. T/R module front-end design example and requirement for mutual coupling technique. Individual control of the TR SWITCH of each element, high isolation of TR SWITCH, and independent beamformers are the essential requirements.

mutual coupling effect (approximately -15 dB) between two adjacent antenna patches, the full transmit power is likely to saturate the receiver of the adjacent element. To provide additional attenuation prior to the receiver, independent front-end switch controls can be utilized. With independent controls, it is possible to utilize the isolation state of the TR SWITCH to provide the attenuation needed.

The mutual coupling measurements are made during the transmit period of the radar timing, and only the short (1 μs) transmit pulse is used for these measurements. As transmit and receive operations occur concurrently, stringent channel-to-channel isolation is required. In normal radar operations, a strong transmit signal is sent through the transmit paths. The same transmit signal can be coupled to the receive channels during that same time period. This on-board crosstalk can often overwhelm the external mutual coupling effect. Therefore, it is critical to investigate the channel crosstalk on board the hardware and the receiver characteristics when developing the mutual coupling calibration technique.

Fig. 4 shows a representative case, transmitting from Element 27 and receiving on Elements 19 and 28. Fig. 2 depicts the physical locations of these elements. Note that both receiving elements are immediately adjacent to the transmitting element, but receiving Element 28 shares a T/R module PCB with 27, while receiving Element 19 is on a different PCB. Each plot in Figure 4 illustrates mutual coupling measurements, the different data points are obtained by configuring the receive element at 64 phase shift and 64 attenuation combinations (4,096 total points). In Fig. 4(a), Element 27 is transmitting at full power and the powers received at Element 28 (on the same PCB) are shown. The receive element is often at or near saturation, and shows poor receiver linearity. Fig. 4(b) shows results from the same transmit/receive pair, but with the transmit power attenuated by 20 dB. Here the linearity is improved, and the receiver is kept out of saturation. Fig. 4(c) repeats the full-power transmission of Fig. 4(a), but receiving on Element 19, which is on a separate T/R module PCB from the transmitting element, thus Element 19 is not affected by on-board crosstalk. Note that in this case, the received power remains well below receiver saturation, and shows much more linear response in both phase and amplitude. The effects of the on-board crosstalk between elements which share a T/R module PCB are notable, with much higher powers seen in the receive channel, and significant decline in receiver linearity. On the other hand, by the virtue of two physically separate PCBs, the crosstalk between channels is eliminated. In this case, it is also possible to transmit full power at each element for this mutual coupling calibration development."

III. LRU Array Calibration

Phased array calibration quantifies the phase and amplitude misalignment between the active elements [10], [11]. The objective of the calibration is to sample each element in the array, and compare the obtained results to identify the differences in excitation and in turn, correct when needed. Phased array calibration can be classified in two main types, initial and in-situ [12], [13]. As the name suggests, initial calibration is the first alignment check performed on the phased array system, whereas in-situ calibration refers to one performed at the installation site. This section focuses on briefly discussing about the implementation initial calibration on the LRU Demonstrator. For the in-situ calibration type, the theory, implementation, and results of mutual coupling-based calibration on the LRU Demonstrator can be found in [6].

A. Initial Calibration (Park-and-Probe)

The initial calibration technique chosen for this work is the park-and-probe method [14], [15]. The calibration of the LRU Demonstrator was conducted employing a near-field (NF) anechoic chamber at the Advanced Radar Research Center (ARRC) at the University of Oklahoma. Moreover, after calibration, the antenna patterns synthesized by the LRU were also scanned using the NF chamber. Figure 5 shows an example of the measured 2D calibrated antenna pattern. The LRU is tapered with a Tayor N-Bar weighting (N=4, -20 dB) and the off-boresight (-15° azimuth and 0° elevation), vertical polarization pattern is shown. First side lobe level (SLL) for both azimuth and elevation cuts are around -20 dB and the cross-pol (red dotted lines) level lower than -34 dB.

B. Embedded Element Pattern and Pattern Prediction

Besides the conventional park-and-probe calibration and beam-steered pattern measurements, another array antenna pattern modeling method was investigated using the LRU. Instead of commanding the array for a specific beam-steered angle and performing NF pattern measurements, the beam-steered pattern can be computed if the embedded element patterns were obtained from the array [16]. The embedded element pattern represents the array pattern when only one element is excited and other elements are parasitically excited by the active element. In contrast to the pattern of an isolated element, the embedded element pattern includes the effect of mutual coupling of the array. The radiated pattern of a

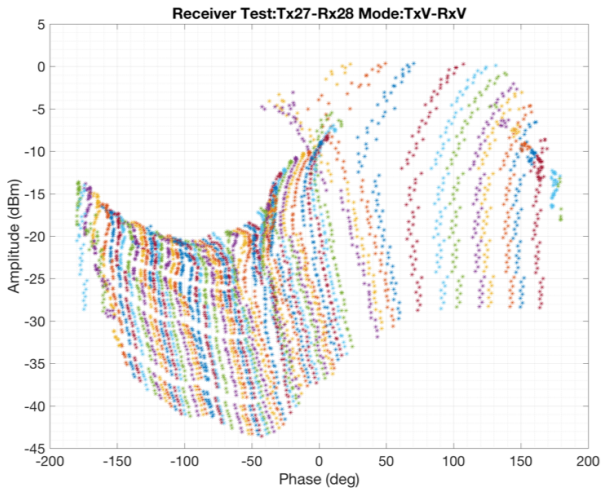

(a)

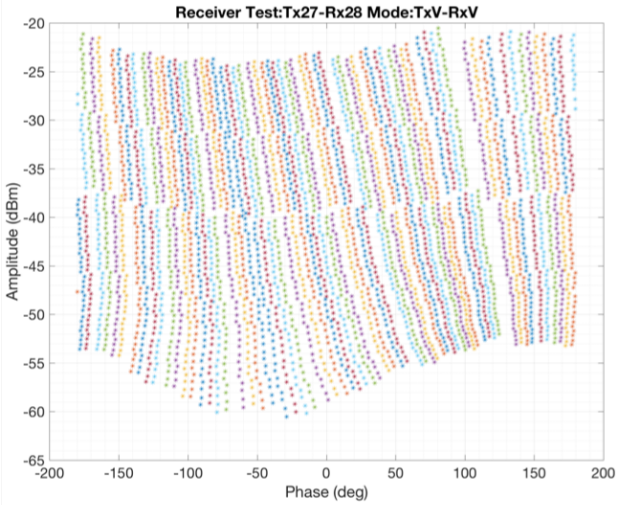

(b)

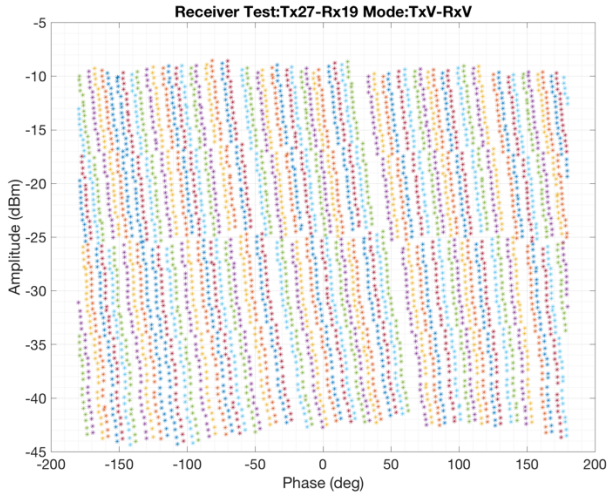

(c)

Fig. 4. Mutual coupling transmitting from Element 27: (a) 4 W transmit, receive on Element 28; (b) 0.04 W transmit, receive on Element 28; (c) 4 W transmit, receive on Element 19.

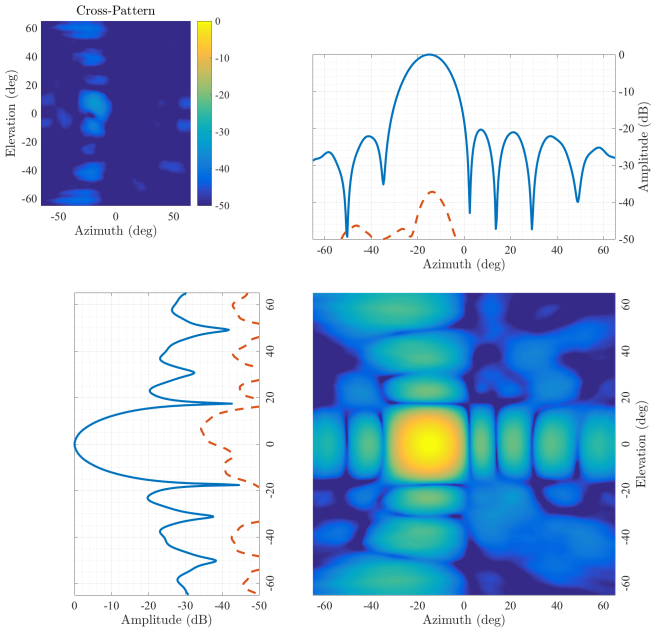

Fig. 5. Example 2D antenna pattern off-boresight. The calibrated vertical polarization pattern applied Taylor N-Bar weighting (N=4, -20 dB). Plotted using Ludwig II definition.

fully excited array can be expressed using superposition of the embedded element patterns. The advantage of the embedded element pattern modeling method is that once all embedded element patterns are measured, any beam-steered pattern can be computed. Details about this testing and calibration methodology can be found in [17].

The azimuth and elevation cuts of the computed and measured patterns are shown in Figure 6. The computed patterns show great agreement with measurements. The corresponding 2D patterns is shown in Figure 7. Again, great similarity is demonstrated. The investigation demonstrates that accurate pattern approximation can be achieved using the embedded element pattern modeling method. This pattern prediction method will provide a much more time-efficient way to investigate beam-steered patterns of an array, compared to the conventional NF method. This promotes the importance of collecting embedded element patterns as part of the phased array initial calibration activities.

IV. Weather Observations

To demonstrate the end-to-end capabilities of the LRU Demonstrator, several weather events were observed during the winter season in Colorado. The Demonstrator was set up at the rooftop of Foothills Lab 1 building (FL1) at NCAR's Foothills campus. The system was set to point northwest to ensure part of the Rocky Mountains' foothills were in the radar range. Table I lists system specification of the LRU Demonstrator. Figure 8 shows a picture of the radar taken during testing on the roof. The LRU Demonstrator provides a half-power beamwidth of approximately 15 degrees. The broad

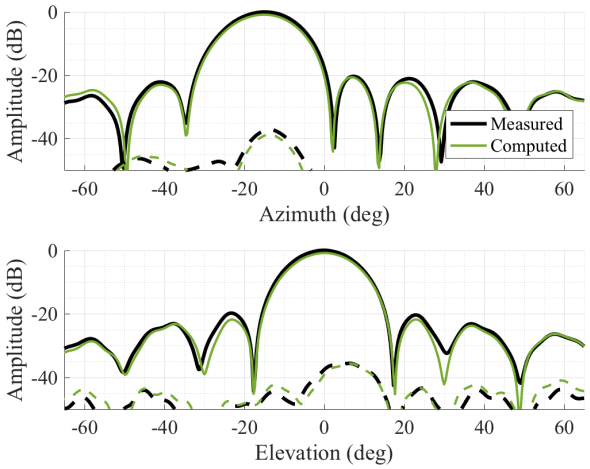

Fig. 6. The off-boresight vertical polarization pattern cuts in azimuth and elevation. The black curves are measured patterns using a NF chamber; the green patterns are computed using the embedded element pattern manipulation method. The dashed lines show the corresponding cross-polarization patterns.

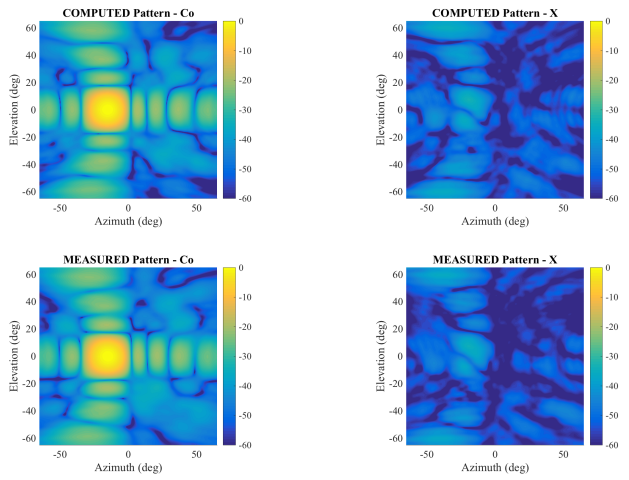

Fig. 7. The vertical polarization 2D patterns. Top figures show computed co-polar and cross-polar patterns; whereas bottom figures depict the corresponding measured patterns using a NF chamber.

beamwidth is driven by the small 64-element size of the array. With this limitation, the sensitivity of the LRU Demonstrator is estimated to be 24 dBZ at 10 km with the NLFM long pulse and pulse compression.

The LRU Demonstrator was configured to perform a fast volume scan over ±45° in elevation and azimuth in approximately 95 s, with a total of 361 beam positions. For each volume scan, the system performed PPI scans in 5° azimuth steps, with a 5° elevation step between each PPI. With the 15° beamwidth, the resolution volume at 5 km is approximately 1.3 km by 1.3 km. This provides a spatial reference for the coarse resolution seen in the PPI scans in Fig. 9. Sample observations of reflectivity (a) and velocity (b) are shown in the figure. Despite the limited sensitivity and coarse spatial resolution, bright echo signatures were observed in reflectivity.

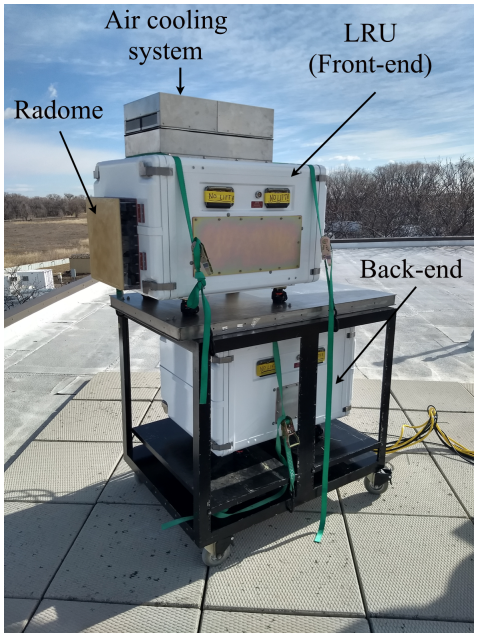

Fig. 8. The integrated LRU-based radar system. The radar system comprises two enclosures: the upper one houses the LRU and the RF transceiver, and the lower one houses the digital transceiver, host computer and power supplies.

The velocity display further distills the types of strong returns – stationary ground clutter with zero velocity (grey) and returns from blizzard with negative velocity (greens and blues) approaching the radar. It is important to note that the large blind zone (6km), colored green in the reflectivity field, is due to the application of long pulse compression; and clutter filtering was employed for all data shown.

TABLE I
SYSTEM SPECIFICATION

Specification	Description
Operating Frequency	5340, 5355 MHz
3 dB Beamwidth	∼15°
Peak Transmit Power	243 Watt
Pulse Repetition Frequency	2 kHz
Pulse Widths	40 µs, 1 µs
Sensitivity	24 dBZ at 10 km NLFM
Dwell Time	500 ms
Scan Spacing	5°in az/el typ.
Volume Scan Duration	95 s

V. CONCLUSION

This paper provides a detailed hardware description of the LRU Demonstrator and the requirements for mutual coupling based (MC) calibrations. While identifying the hardware requirements for the MC calibration techniques, ensuring proper receiver operating region for the MC measurements is extremely critical. The investigation goes through various scenarios between peak transmit power and receiver isolation settings to demonstrate the receiver linearity characteristics.

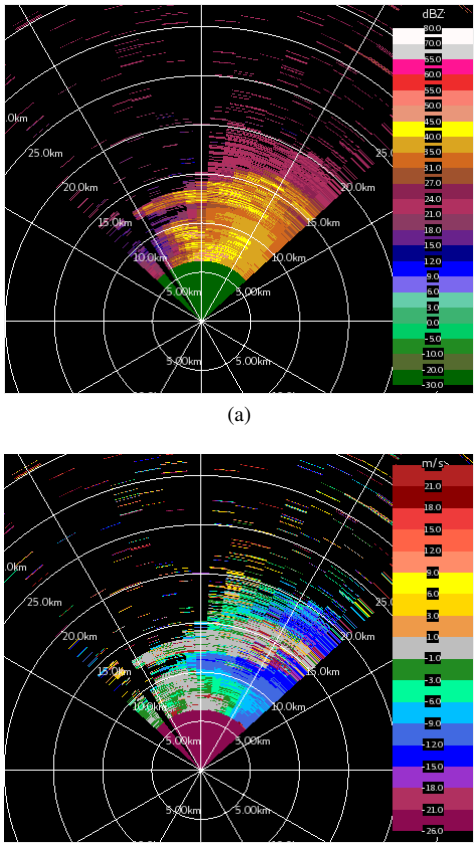

(a)

(b)

Fig. 9. Sample weather observation taken during winter season on March 13, 2019. (a) Reflectivity (uncalibrated) with ground clutter filter enabled; (b)Velocity with ground clutter filter enabled.

The calibration of the LRU Demonstrator is verified using two different methods: initial (park-and-probe) and embedded element pattern prediction. The initial calibration confirms great antenna patterns of the LRU Demonstrator; and the pattern prediction method provides another alternative to evaluate antenna patterns in any beam position. The sample weather observation successfully demonstrates the end-to-end performance of the LRU radar development.

The LRU Demonstrator radar has been an successful development platform for a wide range of PAR related topics. The development exceeds the original vision by implementing fast volume scans, taking results from the initial calibration, beam forming and steering. The volume scan also allows EOL to demonstrate the power of a phased array system – extremely fast update rate and the versatility of scanning. Depending on the constructions of every LRU, the in-situ, fielded MC calibration technique will require continuous, dedicated calibration study to address every unique hardware design and implementation limitation.

REFERENCES

[1] J. Vivekanandan, W.-C. Lee, E. Loew, J. L. Salazar, V. Grubišić, J. Moore, and P. Tsai, "The next generation airborne polarimetric Doppler weather radar," *Geoscientific Instrumentation, Methods and Data Systems*, vol. 3, no. 2, pp. 111–126, 2014.

[2] J. Vivekanandan and E. Loew, "Airborne polarimetric Doppler weather radar: Trade-offs between various engineering specifications," *Geoscientific Instrumentation, Methods and Data Systems*, vol. 7, no. 1, pp. 21–37, 2018.

[3] J. L. Salazar, E. Loew, P. Tsai, J. Vivekanandan, W. C. Lee, and V. Chandrasekar, "Design trade-offs for airborne phased array radar for atmospheric research," in *2013 IEEE PAST*, Oct 2013, pp. 371–378.

[4] E. L. J. Vivekanandan, L. Perez-Clifford and A. Karboski, "Airborne polarimetric doppler phased array weather radar: performance requirements and design specifications," in *2020 IEEE Radar Conference, Florence, Italy*, Sep 2020.

[5] H. M. Aumann, a. J. Fenn, and F. G. Willwerth, "Phased array antenna calibration and pattern prediction using mutual coupling measurements," *IEEE Trans. on Antennas and Propagation*, vol. 37, no. 7, pp. 844–850, 1989.

[6] R. M. Lebrón, P. Tsai, J. M. Emmett, C. Fulton, and J. L. Salazar-Cerreno, "Validation and testing of initial and in-situ mutual coupling-based calibration of a dual-polarized active phased array antenna," *IEEE Access*, pp. 1–1, 2020.

[7] J. L. Salazar, R. H. Medina, and E. Loew, "T/r modules for active phased array radars," in *2015 IEEE Radar Conference (RadarCon)*, May 2015, pp. 1125–1133.

[8] J. L. Salazar, R. H. Medina, and E. Loew, "Transmit/receive (t/r) modules architectures for dual-polarized weather phased array radars," in *2015 IEEE MTT-S International Microwave Symposium*, May 2015, pp. 1–4.

[9] E. L. J. L. Salazar and P. Tsai, "Design and development of a 2-d electronically scanned dual-polarization line-replaceable unit (lru) for airborne phased array radar for atmospheric research," in *2013 36th Conference on Radar Meteorology*, September 2013.

[10] M. A. Salas-natera, R. M. Rodríguez-osorio, and L. D. Haro, "Procedure for measurement, characterization, and calibration of active antenna arrays," *Trans. on Instrumentation and Measurements*, vol. 62, no. 2, pp. 377–391, 2013.

[11] R. H. Medina, J. L. Salazar, E. J. Knapp, and D. J. McLaughlin, "Calibration and validation of the CASA phased array antenna," *European Microwave Week 2012: "Space for Microwaves", EuMW 2012, Conference Proceedings - 42nd European Microwave Conference, EuMC 2012*, pp. 940–943, 2012.

[12] M. G. Sarcione, J. K. Mulcahey, D. Schmidt, K. Chang, M. Russel, R. Enzmann, P. Rawlinson, W. Guzak, R. Howard, and M. Mitchell, "The design, development and testing of the THAAD (theater high altitude area defense) solid state phased array (formerly ground based radar)," in *Internation Symposium on Phased Array Systems and Technology*, 1996, pp. 260–265.

[13] C. Fulton and J. Salazar, "Polarimetric phased array calibration for large-scale multi-mission radar applications," *2018 IEEE Radar Conference (RadarConf18)*, pp. 1272–1277, 2018.

[14] J. K. Mulcahey and M. G. Sarcione, "Calibration and diagnostics of the THAAD solid state phased array in a planar nearfield facility," *Proceedings IEEE PAST*, pp. 322–326, 1996.

[15] I. Şeker, "Calibration methods for phased array radars," *Proceedings of SPIE*, vol. 8714, pp. 87 140W–1 87 140W–15, 2013.

[16] D. F. Kelley, "Array Antenna Pattern Modeling Methods That Include Mutual Coupling Effects," vol. 41, no. 12, pp. 1625–1632, 1993.

[17] R. Lebron, J. D. Diaz, and J. L. Salazar-cerreno, "A procedure to characterize and predict active phased array antenna radiation patterns from planar near-field measurements," in *Annual Meeting and Symposium of the AMTA*, 2018.